Experience-dependent modulation of behavioral features in sensory navigation of nematodes and bats revealed by machine learning

Short Title: Machine learning extraction of behavioral features

Authors: Shuhei J. Yamazaki[1], Yosuke Ikejiri[1], Fumie Hiramatsu[1], Kosuke Fujita[1, 5], Yuki Tanimoto[1, 6], Akiko Yamazoe-Umemoto[1], Yasufumi Yamada[2], Koichi Hashimoto[3], Shizuko Hiryu[2], Takuya Maekawa[4], Koutarou D. Kimura[1*]

Affiliations

[1]Department of Biological Sciences, Graduate School of Science, Osaka University, Toyonaka, Osaka 560-0043, Japan

[2]Faculty of Life and Medical Sciences, Doshisha University, Kyotanabe, Kyoto 6100321, Japan

[3]Graduate School of Information Sciences, Tohoku University, Sendai, Miyagi 980-8579, Japan

[4]Department of Multimedia Engineering, Graduate School of Information Science and Technology, Osaka University, Suita, Osaka 565-0871, Japan

[5]Present address: Department of Ophthalmology, Graduate School of Medicine, Tohoku University, Sendai, Miyagi 980-8574, Japan

[6]Present address: RIKEN Brain Science Institute, Wako, Saitama 351-0198, Japan

*Correspondence: kokimura-lab@umin.ac.jp or kokimura@bio.sci.osaka-u.ac.jp

Classification: Biological Sciences, Neuroscience

ABSTRACT

Animal behavior is the integrated output of multiple brain functions. However, understanding how multiple brain functions affect behavior has been difficult. In order to decipher dynamic brain functions from time-series of behavioral data, we developed a machine learning strategy that extracts distinguishing behavioral features of sensory navigation. We first investigated experience-dependent enhancement of odor avoidance behavior of the nematode *Caenorhabditis elegans*. We segmented worms' trajectories during olfactory navigation into two behavioral states, analyzed 92 features of the states, and automatically extracted 9 distinguishing features modulated by prior odor experience using a statistical index, the gain ratio. The extracted features included ones previously unidentified, one of which indicated that the prior odor experience lowers worms' behavioral responses to a small increase in odor concentration, causing enhanced odor avoidance. In fact, calcium imaging analysis revealed that the response of ASH nociceptive neurons to a small odor increase was significantly reduced after prior odor experience. In addition, based on extracted features, multiple mutant strains were categorized into several groups that are related to physiological functions of the mutated genes, suggesting a possible estimation of unknown gene function by behavioral features. Furthermore, we also extracted behavioral features modulated by experience in acoustic navigation of bats. Thus, our results demonstrate that, regardless of animal species, sensory modality, and spatio-temporal scale, behavioral features during navigation can be extracted by machine learning analysis, which may lead to the understanding of information processing in the brain.

INTRODUCTION

Brain activity can be measured as time series vector data of a large number of neural activities using simultaneous optical monitoring recently (1, 2). Behavior, the integrated output of multiple brain functions such as sensory perception, memory, emotion, and decision-making, however, is still analyzed in classic ways and insufficiently studied using simple and subjectively chosen measures, such as velocity, migratory distance, and/or the probability of reaching to a particular goal. This large asymmetry in data between neural activity and behavior has emerged as one of the significant issues in modern neuroscience (3-5). In other words, without describing when and how behavior changes in detail, we may not be able to fully interpret the meaning of large-scale records of neural activities. One cause for this problem is the difficulty in the analysis of behavior: Although machine-vision techniques over small areas and GPS-based tracking over large areas allow us to continuously monitor the positions and/or postures of animals, it is still unclear which aspects of behavioral features should be focused to clarify the relationships with neural activities.

One way to solve this problem is to use machine learning. Machine learning is a method of extracting latent patterns and discovering knowledge from a large amount of data (6). Machine learning-based behavioral analyses of model invertebrates, such as the fruit fly *Drosophila melanogaster* and the nematode *Caenorhabditis elegans*, have been performed because these model animals are suitable for machine vision monitoring of their behavior due to their small size and relatively simple behavioral patterns (7-13). Furthermore, these animals have relatively small neural circuits, and multiple genetic

72 techniques are available, suggesting that comprehensive analysis of brain function at
73 behavioral, neuronal, and molecular levels is feasible. These analyses have provided
74 new insights into behavioral states and behavioral motifs during voluntary movement,
75 as well as the relationships between optogenetic activation of neurons and behavioral
76 responses. However, machine learning has not been used to understand the brain
77 activity related to sensory behaviors: How is environmental information transformed
78 into behavioral responses through sensory perception and decision-making, as well as
79 its modulation by memory and/or emotion in the nervous system? The lack of research
80 in this topic is likely due to the fact that these invertebrate model animals are too small
81 to accurately and easily measure sensory input during behavior. In addition, even when
82 sensory input can be measured, the method to effectively reveal the dynamic
83 relationships between sensory input and behavioral output has not been established.
84
85 In the present study, we aimed to establish a method to objectively and
86 comprehensively extract behavioral features that are possibly linked to the neural
87 activities for sensory behavior. For that purpose, we analyzed two types of sensory
88 navigation that have been monitored quantitatively but are different in modality and
89 spatio-temporal scale—olfactory navigation of *C. elegans* and acoustic navigation of
90 the bat *Rhinolophus ferrumequinum nippon*—using machine learning. In particular, we
91 focused on experience-dependent modulation (i.e., "learning"; to avoid confusion with
92 machine learning analysis, we do not use this term for biological learning hereafter) of
93 navigation as a model for efficient extraction of differences in behavioral features. In *C.*
94 *elegans*, experience-dependent behavioral modulation has been studied in thermotaxis

95 and salt-taxis, in which worms move in a preferred direction by changing the frequency
96 of directional changes depending on the intensity of the sensory stimulus (14).
97 Consistently, changes in neural activity to a stepwise stimulus change have been
98 revealed by calcium imaging mostly of immobilized worms and in a few cases of freely
99 moving worms (15-20). However, it has not been fully clarified how those behaviors
100 are regulated by neural activity that responds to slight changes in stimuli during
101 navigation in a sensory gradient as well as how the behavioral and neural responses are
102 modulated by experience. Furthermore, although large scale analyses of mutant strains
103 are available (12, 21), methods for effectively analyzing the differences in
104 experience-dependent modulation of sensory behaviors of mutant strains have not been
105 established.
106
107 To reveal experience-dependent modulations of olfactory navigation in worms, we
108 extracted prominent features of behavior and their relationships to odor stimuli using
109 machine learning. For this, we segmented the animals' navigation into two behavioral
110 states and, for individual states, calculated the gain ratio, a statistical index used in
111 decision tree analysis to identify features that distinguish the data in different classes
112 (22). We chose this method because it allows us to easily interpret the results of the
113 analysis for the planning of physiological experiment of neural activities. In the present
114 study, we analyzed 92 features of behavior and sensory information from each of ~200
115 behavioral states of wild-type worms either with or without a prior odor experience (25
116 worms per condition) and found that 9 features are modulated in an
117 experience-dependent manner. One of the extracted features, the reduction in behavioral

118 response to a small increase in odor concentration, was consistent with a change in
119 neuronal activity revealed by calcium imaging. In addition, we calculated gain ratios to
120 identify the experience-dependent changes in olfactory navigation of multiple mutant
121 strains and found that the mutants were categorized into several groups based on
122 behavioral features, which reflect physiological functions of the mutated genes.
123 Furthermore, we also identified experience-dependent modulation of behavioral features
124 from bat acoustic navigation. Thus, we propose that machine learning analysis with gain
125 ratios is an efficient strategy to reveal features of animal behavior in general.
126

127 **METHODS**

128 **Cultivation of worms**

129 The techniques used for culturing and handling *C. elegans* strains have been essentially
130 described previously (23). Wild type Bristol strain RRID:WB-STRAIN:N2_Male and
131 mutant strains RRID:WB-STRAIN:MT1219 *egl-3(n589)*, RRID:WB-STRAIN:VC671
132 *egl-3(ok979)*, RRID:WB-STRAIN:CX4544 *ocr-2(ak47),* RRID:WB-STRAIN:JC1636
133 *osm-9(ky10)*, RRID:WB-STRAIN:JC0570 *tax-4(p678)* were obtained from the
134 Caenorhabditis Genetics Center (University of Minnesota, USA).
135 RRID:WB-STRAIN:KDK1 dop-3*(tm1356)* was originally obtained from National
136 BioResource Project (Japan) and backcrossed five times with N2 .
137

138 **Analysis of worms' olfactory navigation**

139 A 2-nonanone avoidance assay was performed as described previously (24, 25). Briefly,
140 2-3 young adult hermaphrodite worms grown synchronously were placed in the center

141 of a 9-cm nematode growth media (NGM) plate, and 2 μL of 30% 2-nonanone (cat. no.
142 132-04173; Wako, Japan) diluted in EtOH (cat. no. 0057-00456; Wako, Japan) were
143 dropped in two spots on the surface of the NGM plate (Fig. 1A top), and the worms'
144 behavior was recorded for 12 min. This assay was performed under the following three
145 conditions: the worms cultivated on NGM plates with their food bacteria
146 RRID:WB-STRAIN:OP-50 were briefly washed with NGM buffer and subjected to the
147 assay ("naive" condition), or they were subjected to the assay after 1 h of preexposure to
148 0.6 μL of 15% 2-nonanone diluted in EtOH or to only EtOH spotted on the lid of a
149 NGM plate without food ("preexp" and "mock" conditions, respectively). We added the
150 mock-treated control to confirm that 1-h starvation did not affect the odor avoidance
151 behavior of worms and to extract behavioral features modulated by the odor
152 preexposure compared to the naive and the mock-treated controls. Images of worms the
153 NGM plate during odor avoidance assay were acquired by a high-resolution USB
154 camera (DMK 72AUC02; The Imaging Source, USA) with a lens (LM16JC5MW;
155 Kowa, Japan) at 1 Hz for 12 min. From the recorded images, the coordinates of
156 individual animals' centroids were acquired using Move-tr/2D software (Library Co.,
157 Ltd., Tokyo, Japan) and used for the following analysis.
158
159 Similar to worms' other sensory behaviors, trajectories in the 2-nonanone avoidance
160 assay can be divided into two states: "run", a relatively long period of straight
161 movement, and "pirouette", a period of short movements interrupted by frequent
162 reversals and turns (24, 26). Angular change per s was calculated from the centroid
163 coordinates, and movements of 1 s with angular change larger than 90° were classified

164 as a turn. A histogram of turn intervals was fitted by two exponentials, suggesting that
165 turn intervals are regulated by two probabilistic mechanisms (25, 26). The time of the
166 intersection of the two exponentials was defined as t_{crit}, and turn intervals longer or
167 shorter than the t_{crit} were classified as runs or included in pirouettes, respectively. t_{crit}
168 was calculated for the control (i.e., naive plus mock-treated) condition for wild-type and
169 mutant strains, respectively. In this study, we analyzed features of runs but not of
170 pirouettes except for their duration because pirouettes appear to have little effect on
171 odor avoidance (25). Excel 2010 (Microsoft Corp.) was used for these calculations. The
172 odor concentrations that worms experienced at specific spatio-temporal points were
173 calculated according to the dynamic odor gradient model based on the measured odor
174 concentration (19).
175
176 **Bats**
177 As previously described, three adult Japanese horseshoe bats (*Rhinolophus*
178 *ferrumequinum nippon*, body length: 6.0–8.0 cm, body mass: 20–30 g) were captured
179 from natural caves in Hyogo and Osaka prefectures in Japan (27). The bats were housed
180 in a temperature- and humidity-controlled colony room [4 (L) × 3 (W) × 2 m (H)] with
181 a 12-h-on/12-h-off light cycle at Doshisha University in Kyoto, Japan. The bats were
182 allowed to fly freely and given access to mealworms and water. Captures were
183 conducted under license and in compliance with current Japanese law. All experiments
184 complied with the Principles of Animal Care, publication no. 86-23, revised 1985, of
185 the National Institutes of Health, and with current Japanese law. All experiments were
186 approved by the Animal Experiment Committee of Doshisha University.

Bat acoustic navigation

Methods for acoustic navigation measurement in bats have been described elsewhere (Yamada et al., in revision). In brief, the experiments were conducted in a flight chamber, which was constructed of steel plates [9 (L) × 4.5 (W) × 2.5 m (H)] under lighting with red filters (>650 nm) to avoid visual effects on the bats. An obstacle environment was constructed using plastic chains (4 cm in diameter) that were suspended from the ceiling of the chamber. The chains were arranged at 15-cm intervals in the *x*-axis and at 22-cm intervals in the *y*-axis so that the bat was forced to fly in an S-shaped pattern without passing between chains. With this layout, three naive bats were used: each bat was observed for 12 continuous repeated flights so that echolocation behaviors in unfamiliar and familiar spaces could be compared. In this study, the initial three flights were defined as unfamiliar flights, and the last three flights were defined as familiar flights.

The flight behavior of the bats was recorded using two digital high-speed video cameras (MotionPro X3; IDT Japan, Inc., Japan) at 125 frames/s, which were located in the left and right corners of the flight chamber. Based on a direct linear transformation technique, the successive 3D positions of the flying bats, as well as the locations of other objects, were reconstructed using motion analysis software (DIPPMotionPro ver. 2.2.1.0; Ditect Corp., Japan). The flight velocity vector of the bat was calculated as the time derivative of the coordinates of its flight trajectory.

Behavioral parameters included in a feature vector

For the machine learning analysis of worm olfactory navigation, the following behavioral features were calculated for each run from the centroid coordinates of the worms: start time (*RunTime*), serial number (*RunNum*), velocity (*V*), bearing (*B*), odor concentration that a worm experienced during run (*C*), directionality ratio (*Dir*) (28), run's curvature (called weathervane; *WV*) (29), run duration (*RunDur*), and duration of pirouette just before the run (*PirDur*). Time-differential values were calculated for *V* (*dV*), *B* (*dV*), and *C* (*dC*). For these values, the average (*Ave*) during a run as well as average values over 2 s at the initiation (*Ini*) and at the termination (*Ter*) of a run were also calculated. For *Ini* and *Ter*, 0-2 s after the initiation and 2-4 s before the termination of a run were used; we did not use 0-2 seconds before the termination because previous studies revealed that a worm's speed drops largely during this period (25, 26). Although the time windows for worms were set based on the previous studies, the optimal time windows for bats were calculated by machine learning (see below). In addition, to analyze whether these features are independent for each run (in other words, whether any long-term trend among runs across a pirouette exists), we also calculated hysteretic effects (Δ) of these run features between successive runs for *V*, *dV*, *B*, *dB*, *C*, and *dC*—in fact, a certain relationship between bearings before and after a pirouette (*B_Ini*Δ*Ter*) has been reported in salt-taxis (26). For this, *Ave*, *Ini,* or *Ter* of each run feature was subtracted from any of the previous run features. Hysteretic effects were calculated for just one feature for *RunDur*, *PirDur*, and *WV*, which only possess one value per run, and not calculated for *RunTime* and *RunNum*. A total of 92 features were calculated by combining all these features.

For analysis of changes in the flight of the bats, the following behavioral features in each flight were calculated from the coordinates of the animals and obstacles: three-dimensional flight velocity (*V*), horizontal and vertical bearings of the flight (*B_hori* and *B_vert*, respectively), distance (*R_obs*) and bearing (*B_obs*) of the bat to the nearest edge point of the obstacle chain array, longitudinal directional distance to the frontal chain array (*R_x*), lateral directional distance to the inside pitch of the chain array (*R_y*). Time-differential values were calculated for *V* (*dV*), *B* (*dB*), *dB* (*ddB*), and the flight height (*dH*), which were calculated with frame units of the high-speed video cameras (1/125 s). All flight trajectories were divided into three segments: earlier, middle, and later terms. The time window for the analysis of each behavioral feature was 0.1, 0.2, or 0.3 s before or when ($t = 0$) passing through the chain array. A total of 42 features were calculated by combining all these features.

Excel 2010 and Visual C# (Microsoft) were used for the calculations, and the Beeswarm package for R software (The R Project) was used for the scattered plot of data. These parameters are listed in Table 1 for worms and in Table 4 for bats.

Behavioral classification with gain ratio

In order to extract useful features, we calculated the gain ratio used in C4.5 decision tree analysis (30) for each feature. In decision tree analysis, the amount of information, which is acquired when a group of data is divided into sub-groups by a certain feature, is calculated as information gain. In other words, when dividing a group into sub-groups

256 by applying a certain feature, information gain is an index indicating the amount of the
257 increased bias of data in the sub-groups after the division. The information gain was
258 then divided by split info, a degree of division, for normalization to compute the gain
259 ratio. For worm olfactory navigation, we extracted behavioral features that have positive
260 gain ratios in naive versus preexposed worms or in mock-treated versus preexposed
261 worms. Then, we chose the features that were common in both comparisons as "features
262 modulated in experience-dependent manner". For bat acoustic navigation, behavioral
263 features were extracted from the comparison of unfamiliar flights (1st-3rd) and familiar
264 (10th-12th) flights. Weka software (the University of Waikato, New Zealand) (31) was
265 used for the calculation.
266
267 **Calcium imaging**
268 Calcium imaging of the worms' ASH neurons was performed according to a previous
269 report (19). Briefly, transgenic strains expressing GCaMP3 (32) and mCherry (33) in
270 ASH sensory neurons under the *sra-6* promoter (KDK70034 and KDK70072; 20 ng/µl
271 of *sra-6p::GCaMP3*, 20 ng/µl of *sra-6p::mCherry*, 10 ng/µl of *lin-44p::GFP*, 50 ng/µl
272 of PvuII-cut N2 genomic DNA as a carrier in N2 background) were placed on an NGM
273 agar plate on a robotic microscope system, OSB2 (19). Although these transgenic
274 worms were immobilized with the acetyl choline receptor agonist levamisole (34) for
275 high-throughput data acquisition by simultaneous imaging of multiple worms, the
276 previous study revealed that the ASH activity is essentially unaffected by
277 levamisole-treatment (19). For these worms, a constant gas flow of 8 mL/min was
278 delivered, in which the mixture rate of 2-nonanone gas versus the air was changed to

279 make a temporal gradient of the odor concentration. The temporal change in odor
280 concentration was measured by a custom-made semiconductor sensor before and after
281 the series of calcium imagings on each day. The fluorescence signals of GCaMP3 and
282 mCherry in ASH neurons were divided into two channels using W-View (Hamamatsu,
283 Japan), an image splitting optic, and captured by an EM-CCD camera (ImagEM;
284 Hamamatsu, Japan) at 1 Hz. The intensities of fluorescence signals from cell bodies
285 were extracted and quantified by ImageJ (NIH) after background subtraction. The
286 average ratio over 30 s prior to the odor increase was used as a baseline (F_0), and the
287 difference from F_0 (ΔF) was used to calculate the fluorescence intensities of GCaMP3
288 and mCherry ($F = \Delta F/F_0$). The ratio between florescence intensities of GCaMP and
289 mCherry (GCaMP/mCherry) was used in the figure.
290
291 **Statistical analysis**
292 For comparisons of behavioral features among naive, mock-treated, and preexposed
293 worms, the Kruskal-Wallis multiple comparison test followed by the *post hoc* Dunn's
294 test were used (Fig. 2, 3 and 4), except for in the analysis of directional data, for which
295 the Mardia-Watson-Wheeler test was used. The calculations were performed with Prism
296 ver. 5.0 for Mac OSX (GraphPad Software, CA, USA), R (The R Project) or SPSS
297 version 23 (IBM Corp.).
298
299 **RESULTS**
300 **A strategy for extracting features of sensory navigation that were modulated by**
301 **prior experience**

302 In this study, we aimed to extract behavioral features using machine learning to
303 understand changes in information processing in the brain during sensory navigation.
304 However, identifying characteristic changes in behavior and sensory stimulus during
305 navigation has been difficult. It is because sensory stimulus in general changes
306 gradually and continuously during navigation, which may cause gradual or sudden
307 response at some aspects of behavior with certain probabilities. In order to efficiently
308 extract behavioral features of sensory navigation by machine learning, we considered
309 the following points for the analysis: (1) segmenting behavioral states, (2) representing
310 the animal's position as a single point, (3) calculating sensory information, and (4) using
311 a statistical index, gain ratio.
312
313 ***Segmenting behavioral states***
314 Segmentation is one of the important preprocessing steps of a large dataset for effective
315 analysis (35).We considered an animal's navigation to be a series of transitions among a
316 limited number of behavioral states for a certain period, and we analyzed features in
317 each of the behavioral states instead of analyzing features in an entire navigation
318 trajectory or in very short temporal unit (i.e., second or sub-second). For worm
319 olfactory navigation, we segmented the navigation into two well-established behavioral
320 states: runs and pirouettes (14, 26; see METHODS for details). For bat acoustic
321 navigation, we considered the period from passing one obstacle (or from the starting
322 point) until passing the next obstacle as one behavioral state.
323
324 ***Representing animal's position as a point***

325 During a behavioral state in navigation, animals move a certain distance. For the sake of
326 proper dimensionality reduction, we calculated the trajectories of a point representing
327 animal's position (centroid for worms and head position for bats), instead of the posture
328 of an animal, whose description requires more detailed spatial and temporal
329 information.
330
331 ***Sensory information***
332 Sensory information is a key factor affecting an animal's behavior. However, because
333 of technical difficulties, it has been included in the analysis of sensory navigation only
334 in a few cases for small model animals (17, 19, 36). We included the information of
335 odor concentration, which changes dynamically during navigation of worms, as
336 revealed by the direct measurement of odor concentrations in specific spatio-temporal
337 points in a behavioral arena (19).
338
339 ***Gain ratio***
340 To comprehensively examine behavioral features that can be modulated by prior
341 experience, we focused on a statistical index used in machine learning-based
342 classification analysis. In general, classification analysis is the task of classifying new,
343 unlabeled data into appropriate classes using characteristic features and their parameters
344 that have been extracted from the known class-labeled data. In the present study,
345 however, the classification itself was not meaningful because the data were already
346 classified, such as with or without prior experience or wild-type versus mutant strains.
347 Instead, we focused on the procedure in the classification that finds features useful for

348 distinguishing between the two classes. In other words, behavioral features modulated
349 by prior experience should be able to effectively classify the behavioral data of animals
350 with or without this experience.
351
352 For this purpose, we chose to use gain ratio, the index for decision tree analysis (22).
353 Binary decision tree analysis is performed to split a data set into two sub-groups by
354 automatically selecting the best feature and its parameter that has the largest
355 information gain, the difference of the uncertainty ("information entropy") before and
356 after division; each data point is classified into either of the sub-classes based on
357 whether it has a larger or smaller value than the threshold. When applied for binary
358 classification, decision tree analysis automatically evaluates the classification
359 performance of all of a large number of features that are designed by the researchers.
360 The result of this analysis is the extraction of certain features, which allows us to easily
361 understand the usefulness of particular features for the classification. This is a
362 substantial difference from the analysis by support vector machines and/or deep neural
363 networks, where the relationships between features of the data and the classification are
364 not easily discernible (see DISCUSSION).
365
366 **Behavioral features modulated by the prior experience in worm odor avoidance**
367 **behavior**
368 We analyzed the experience-dependent enhancement of odor-avoidance behavior of *C.*
369 *elegans* as a model. We have reported that preexposure of worms to the repulsive odor
370 2-nonanone causes enhancement of avoidance behavior to the odor. After 1 h of

371 preexposure, worms migrate farther away from the odor source as a type of
372 non-associative middle-term learning (24). A series of genetic analyses indicated that
373 neuropeptide and dopamine signaling pathways are required for acquisition and
374 execution of the odor memory, respectively (25), suggesting that this non-associative
375 middle-term memory is caused by a circuit-level modulation of neural activity rather
376 than simple sensory sensitization.
377
378 Previous studies analyzed several features and revealed that run duration is the major
379 behavioral change caused by odor preexposure, likely because of reduction in the
380 pirouette initiation rate (24, 25). However, this did not rule out the possibility that other
381 behavioral features play more profound effects. Moreover, multiple mutant strains
382 exhibit their own abnormalities in the enhanced odor avoidance behavior (see below),
383 although identification of the features modulated in each mutant strain is
384 time-consuming and laborious. To reveal features modulated by prior experience
385 comprehensively and effectively, we calculated the gain ratio by comparing naive
386 versus preexposed and mock-treated versus preexposed animals, and we considered
387 features that were extracted from both comparisons.
388
389 In the machine learning analysis, we calculated gain ratios of 92 features (Fig. 1 and
390 Table 1; see METHODS for details) and extracted 18 and 15 features from the
391 comparisons of naive versus preexposed and mock-treated versus preexposed worms,
392 respectively (Table 2). Nine features were shared between the two comparisons,
393 suggesting that those features were modulated by the prior experience to cause the

394 enhanced odor avoidance (Table 2 and Fig. 2A). These features are related to run
395 duration (*RunDur*), temporal differences in bearing (*dB_X*), odor concentration (*C_X*),
396 and its temporal difference during runs (*dC_X*). Modulation of run duration (*RunDur*;
397 Fig. 2B) by the prior odor experience was previously revealed by traditional analysis
398 (24). Thus, this result supports the validity of the machine learning analysis.
399
400 Experience-dependent modulations of temporal differences in bearing (*dB_X*; Fig. 2C
401 for example and Table 2) have not been revealed previously. Its contribution to the
402 enhancement of avoidance distance, however, are unclear. Differences between the
403 average or the terminal bearing change and the previous initial value (*dB_Ave*Δ*Ini* or
404 *dB_Ter*Δ*Ini*) were also extracted (Table 2), while the differences were likely due to the
405 modulation in the previous initial value (Δ*Ini*), not due to the change in hysteretic
406 effects.
407
408 Odor stimuli during runs, which likely drive the worms' odor avoidance behavior, were
409 also found to be modulated in several aspects: the initial, terminal, and average odor
410 concentration (*C_Ini*, *C_Ter*, and *C_Ave*), and the terminal and average odor
411 concentration change (*dC_Te*r and *dC_Ave*) (Table 2; Fig. 2D and E for *C_Ave* and
412 *dC_Ave*, respectively, for examples). However, this result does not directly imply that
413 the lower odor concentration is the causal reason for the enhanced avoidance distance;
414 one possible scenario is that, because the odor-experienced worms were located farther
415 away from the odor source, they sensed a lower concentration of the odor.
416

417 Because the terminal and average values of odor concentration change (*dC_Te*r and
418 *dC_Ave*) were extracted, and because a previous study demonstrated that worm odor
419 avoidance behavior depends on *dC*, rather than *C*, at least in naive conditions (19), we
420 investigated these features more in detail. We compared ensemble averages of *dC/dt*
421 that worms sensed during the last 30 s of each run (Fig. 2F). Interestingly, although
422 most of the control (*i.e.* naive and mock-treated) worms sensed 2-3 μM odor
423 concentrations (Fig. 2D), *dC/dt* at the end of each run was ± 0.1 nM/s on average (Fig.
424 2F; 0.09 ± 0.72 and -0.09 ± 0.76 nM/s for naive and mock-treated animals, respectively).
425 This result suggests that, to initiate a pirouette, worms respond to a subtle odor
426 concentration change, of which the magnitude is 1/20,000 - 1/30,000 of the odor
427 concentration itself per second. Even considering that sensory information is temporally
428 integrated for a few seconds during worm chemosensory navigation (19, 37), this value
429 is far lower than the general psychological threshold for sensory signals: The lower
430 threshold of signal change (ΔS) is more than 1/100 of the signal intensity (S) (38).
431
432 This extreme sensitivity to positive *dC/dt* was modulated by prior experience of the
433 odor. The terminal *dC/dt* was significantly higher than in naive and mock-treated
434 animals (1.58 ± 0.6 nM/s compared to the values in the previous paragraph; $p < 0.01$,
435 the Kruskal-Wallis multiple comparison test followed by the *post hoc* Dunn's test). This
436 change in terminal *dC/dt* could be the cause for the enhanced odor avoidance behavior
437 and suggest the following model: the worms without prior experience of the odor are
438 highly sensitive to a slight increase in odor concentration during a run, which is a sign
439 of inappropriate movement toward the source of the repulsive odor, and they respond to

440 it by initiating a pirouette. In contrast, the worms with prior odor experience ignore the
441 slight odor increase and continue the run, which leads to a longer run duration (Fig.
442 2G).
443
444 **The responsiveness of sensory neurons to odor increases was modulated by odor**
445 **experience**
446 If the change in sensitivity to positive *dC/dt* is the causal reason for the enhanced odor
447 avoidance behavior, it should be associated with changes in neural activity. Thus, we
448 analyzed the responsiveness of a likely candidate group of neurons, ASH nociceptive
449 neurons (39, 40). Previously we established the OSB2 microscope system that allows
450 for calcium imaging of *C. elegans* neurons *in vivo* under odor stimuli resembling ones
451 that worms experience during the odor avoidance assay in the plates (19). Using the
452 OSB2 system, we found that ASH neurons are the major sensory neurons to cause
453 pirouettes upon increases in 2-nonanone concentration (19). However, whether the ASH
454 response is modulated by 2-nonanone experience has not been studied.
455
456 We found that ASH responses were modulated by prior odor experience in a manner
457 consistent with the behavioral modulation. When the worms were stimulated with 5
458 nM/s odor increase, which is the lowest rate of change to cause the threshold-level
459 behavioral response in the previous study (19), ASH neurons in naive as well as
460 mock-treated worms exhibited robust responses (Fig. 3A and B). However, the ASH
461 responses were significantly reduced in the preexposed animals (Fig. 3B and C). This
462 result suggests that prior odor experience causes the reduced response to the odor

463 increase, which causes longer run durations and enhanced odor avoidance behavior.

464

465 **Extracted behavioral features of mutant strains correspond to gene functions**

466 We also investigated whether feature extraction from behavior of mutant strains can
467 allow us to understand relationships between chemosensory behavior and gene
468 functions in the nervous system. By calculating gain ratios, we analyzed mutants of
469 genes that are known to be involved in the experience-dependent modulation of
470 2-nonanone avoidance behavior, such as that for proprotein convertase (required for
471 neuropeptide signaling), EGL-3 (41), and the D2-type dopamine receptor DOP-3 (25,
472 42), as well as genes involved in sensation of chemical signals, such as those for TRP
473 channel homologs OCR-2 and OSM-9 (43, 44) and the cGMP-gated cation channel
474 TAX-4 (45), whose relationships to the 2-nonanone avoidance behavior have not been
475 studied.

476

477 *egl-3*, encoding a homolog of proprotein convertase, is required for neuropeptide
478 biosynthesis, expressed in many neurons, and known to be involved in various aspects
479 of worm behavior including learning (25, 41, 46). Deletion and missense mutations of
480 the gene are known to cause severe and mild phenotypes, respectively (25, 47). Our
481 previous study revealed that run duration is not increased after preexposure in *egl-3*
482 mutants, suggesting that neuropeptide signaling is required for the acquisition of odor
483 preexposure memory (25). In the present study, the abnormal features were similar
484 between deletion (*ok979*) and missense (*n589*) mutants, namely, run duration
485 (*Run_Dur*), odor concentration (*C_Ave*, *C_Ini*, *C_Ter*), and odor concentration change

486 (*dC_Ave*, *dC_Ter*), although the deletion mutants exhibited additional abnormal
487 features (Table 3 and Fig. 4). Increases in odor concentration in preexposed worms were
488 interesting because they were observed only in *egl-3* mutants but not in any other
489 mutants.
490
491 Mutations in *dop-3*, which encodes a homolog of the D2-type dopamine receptor, were
492 previously found to affect migratory direction after preexposure (25). This was
493 concluded because the mutants did not exhibit enhanced avoidance distance, although
494 run duration was increase after preexposure, and because run terminal bearing (*B_Ter*)
495 was worsened (25). These features were extracted in this analysis (Table 3), further
496 supporting the reliability of this analysis. In addition, the averaged directionality ratio
497 (*Dir_Ave*) was worsened (Table 3 and Fig. 4C). This is also consistent with the idea that
498 migratory direction is worsened in *dop-3* mutants after preexposure. Moreover, lowered
499 velocity (*V_Ave*, *V_Ter*; Table 3 and Fig. 4B) was also extracted, which may also
500 contribute to the failure in the enhanced odor avoidance. Such multiple abnormal
501 phenotypes are consistent with the fact that *dop-3* is expressed in many neurons and
502 involved in the regulation of multiple aspects of behavior (48).
503
504 *ocr-2* and *osm-9* both encode homologs of TRP-type cation channels, expressed in
505 multiple sensory neurons including ASH neurons and considered to be involved in
506 sensory perception as well as its modulation (43). We found that mutants for these two
507 genes did not exhibit significantly enhanced odor avoidance (Fig. 4A). In addition,
508 these mutants exhibited increases in velocity (*V_Ave* and *V_Ter*) after preexposure,

509 which was specific for these two mutants but not observed in other mutants. Some
510 features are specific for each mutant strains, which may reflect the differences in their
511 expression and/or function (43). Mutants of *tax-4*, encoding a homolog of the
512 cGMP-gated cation channel expressed in different sets of sensory neurons, exhibited a
513 unique pattern of features (Table 3, Fig. 4).
514
515 Taken together, our results suggest that the pattern of extracted features from mutant
516 strains may reflect functional groupings of the mutated genes. Thus, profiling and
517 classification of extracted mutant features of unknown genes may be useful to estimate
518 their physiological functions.
519
520 **Feature extraction of experience-dependent modulation of acoustic navigation of**
521 **bats**
522 To demonstrate the general applicability of our method, we examined features of
523 acoustic navigation in bats. We have previously reported that bats improve their flight
524 trajectory in an indoor space with obstacles in an experience-dependent manner
525 (Yamada et al., in revision). Here, we analyzed 42 features using gain ratios and
526 extracted several features, such as velocity (*V*), distance to the obstacle chain array
527 (*R_obs* and *R_x*), and horizontal bearing of the flight (*B_hori*) (Table 4 and Fig. 5A-C).
528 Interestingly, although velocity (*V*) itself was modulated by flight experience,
529 acceleration (*dV*) was not (Fig. 5D), suggesting that bats may determine flight speed
530 before initiating but not during navigation, at least in our experimental conditions.
531 Because the bats' vocalizations reflect their attention or decisions (49), our results

532 suggest that such higher brain functions during navigation could be extracted by
533 machine learning analysis.
534
535 **DISCUSSION**
536 In the present study, we extracted behavioral features that are modulated by experience
537 from olfactory navigation of worms and from acoustic navigation of bats using machine
538 learning analysis. In the case of worm olfactory navigation, we found a neural correlate
539 for one of the newly identified features: The reduced behavioral response to an increase
540 in odor concentration was consistent with the reduced response of ASH nociceptive
541 neurons to a small increase in odor concentration. In addition, we also found that mutant
542 strains can be grouped based on extracted features, which may correspond to the
543 physiological roles of genes in chemotaxis and/or experience-dependent modulation.
544 Furthermore, our machine learning analysis was applied to acoustic navigation of bats
545 to extract the features modulated by prior experience.
546
547 **Extraction of behavioral features by machine learning**
548 Machine learning has been playing a major role in classifying behavioral data of model
549 animals into several categories (7-13, 50). Instead of such behavioral classification,
550 however, we intended to use a machine learning technique for extracting characteristic
551 features of sensory behavior to decipher information processing in the brain. For that
552 purpose, we first hypothesized that a change in a behavioral feature reflects a change in
553 activity of a functional unit of the brain. Then, we used machine learning to extract
554 behavioral features that differ between two classes of behavior, rather than to categorize

555 the behavioral data into two classes; in our study, two classes (e.g., "with or without
556 prior experience" or "wild-type versus mutant strains") were determined *per se* and did
557 not need to be categorized.
558
559 In addition, we also included sensory information that worms experienced during the
560 course of behavior in the machine learning analysis. Although small model animals
561 such as *C. elegans* or *Drosophila melanogaster* are suitable for machine vision
562 monitoring and subsequent quantitative analysis of behavior, their small size makes it
563 difficult to measure sensory signals they receive during behavior. We have solved this
564 problem by precisely measuring the odor concentration at multiple spatio-temporal
565 points in a paradigm to assess olfactory behavior of worms (19), which allowed us to
566 include the information of odor concentration and its temporal changes (*C* and *dC*) into
567 the feature vector for the machine learning analysis. Our machine learning method
568 could also be used for detailed analysis of sensory navigation in the environment where
569 the gradients of chemical signal were also quantitatively monitored (36, 51, 52).
570
571 As a result, we were able to find multiple behavioral features modulated by prior
572 experience, including the temporal odor concentration change (*dC_Ter*), which was
573 consistent with the experience-dependent change in the responsiveness of ASH
574 nociceptive neurons. Such an effective and objective approach to estimate neural
575 function from comprehensive behavioral analysis may play important roles in the
576 understanding of recent large-scale monitoring of neuronal activity (see below).
577

578 For machine learning-based classification, support vector machines and deep learning
579 have also been used (53, 54). However, in these analyses, it is difficult for researchers
580 to understand which features are characteristic to each group because these algorithms
581 attempt to combine multiple features in a single representation. In other words, it is
582 difficult to use the results of classification for subsequent experiments and/or analysis to
583 further investigate the neural correlates of the behavioral differences. In contrast, in the
584 calculation of gain ratio, all features are evaluated independently, allowing us to
585 immediately translate the results of analysis to a new understanding and/or hypothesis
586 for subsequent experiments and analyses, as shown in the present study. Thus, we
587 conclude that the method used in this study—making a list of characteristic features
588 based on gain ratios and subsequently performing detailed analyses on each of extracted
589 features—is effective to understand the basic principles of neural functions regulating
590 behavior.
591
592 However, causal relationships among extracted features should be considered carefully.
593 For example, because odor concentration (*C*) and temporal odor concentration change
594 (*dC*) are both features of sensory stimuli, they were likely candidates for the cause of
595 changes in behavioral response. However, we regard that *dC*, rather than *C* itself, is the
596 causal reason because of the following: (1) previous quantitative analysis in the plate
597 assay paradigm revealed that pirouettes and runs are strongly correlated with positive or
598 negative *dC*, respectively, rather than the value of *C*; (2) in the OSB2 robotic
599 microscope system, positive or negative *dC* caused high or low levels of turning, such
600 as pirouettes and runs, respectively (19). For example, the lower *C* in preexposed

601 worms is likely caused by their relatively lower positions in the odor gradient (i.e.,
602 farther positions from the odor source) caused by the enhanced avoidance behavior. In
603 other words, sensory behaviors are closed loops—changes in sensory input cause
604 changes in behavior, while changes in behavior should also cause changes in sensory
605 input because the positions and/or directions of sensory organs are changed due to the
606 behavior. Thus, even when sensory features are extracted by machine learning, causal
607 relationships with behavioral features should be evaluated by independent experiments:
608 An open loop system, which allows control of sensory stimuli and monitoring behavior
609 independently, such as the OSB2 system (19), will provide an effective solution.
610
611 Analysis of multiple mutant strains revealed that the extracted features appeared to be
612 correlated with the physiological roles of the genes. For example, two alleles of a gene
613 required for neuropeptide signaling (*egl-3*) exhibited similar feature patterns, which
614 were different from mutants of a dopamine-signaling gene (*dop-3*). In addition,
615 mutations in two homologous but distinct TRP-type channel genes required for sensory
616 signaling (*ocr-2* and *osm-9*) exhibited a similar feature pattern, and the one for cyclic
617 nucleotide-gated ion channels (*tax-4*) exhibited a different pattern. It is interesting that
618 mutants of genes with similar functions exhibited similar behavioral features although
619 these genes should influence animal behavior in a complex manner. These results
620 suggest that behavioral features of mutants of a novel gene may be categorized to a
621 group of genes which have similar physiological functions. In other words, feature
622 extraction using gain ratio of multiple mutant strains can allow estimation of gene
623 functions in the nervous system.

In conclusion, we established a machine learning method to effectively reveal different features of two different sensory behaviors. In particular, it is important to include not only the behavior itself but also environmental sensory information that animals sense in the feature vectors. Furthermore, it is also necessary to verify causal relationships of the extracted features by other methods, such as using an open loop experimental setup. In addition, this method can be used for estimation of the physiological function of genes.

This method could be applied to analysis of more complex behaviors of other animals. In the case of visual and acoustic stimuli, it is not clear what features of the stimuli (e.g., shapes, colors, and brightness for visual stimuli, and frequency and intensity for acoustic stimuli) have the most prominent effects on behavior in a particular context. We believe that our method presented herein, which allows extraction of the essential features of information processing for sensory behaviors in the brain in an objective and comprehensive manner, will help to solve this problem. Poor description of behavior with simple indices compared to "big data" on neuronal activity is being recognized as one of the significant problems in modern neuroscience (3-5). We expect that comprehensive and objective feature extraction would increase the wealth of description of behavior, which will provide us clues to understand more of the big data from brain activity monitoring.

FIGURE LEGENDS

647 Figure 1. A workflow of the machine learning method for the analysis of worm odor
648 avoidance behavior; "Behavioral data" (Top) Examples of the trajectories of 3 worms
649 during 12 min of 2-nonanone avoidance assay, overlaid on a schematic drawing of a
650 9-cm agar plate. (Second from the top) A magnified view of trajectories of a worm, in
651 which runs are blue and pirouettes are red. (Second from the bottom and bottom)
652 Graphs showing the odor concentration (*C*, second from the bottom) and temporal
653 changes in *C* (*dC*, bottom) at the worm's position at 1-s intervals during the odor
654 avoidance assay. "Feature vector" From the (*x*, *y*) coordinates of each worm's centroid,
655 velocity, bearing, odor concentration, and their derivatives (*V*, *B*, *C*, *dV*, *dB*, and *dC*) as
656 well as the difference between the present and the previous values (Δ) were calculated.
657 "Gain ratio" One example (*C_Ter*) of calculating gain ratio is shown.
658
659 Figure 2. Extracted features that were modulated by prior experience of the odor. (A)
660 Enhanced odor avoidance behavior of worms caused by odor preexposure. (Left) End
661 points of 25 worms in each condition plotted on a schematic drawing of the assay plate.
662 (Right) Avoidance distance (distance between the center line of the plate and end point
663 of behavior) of each worm. Each bar represents median. Significant differences were
664 observed in the preexposed worms compared to the naive and mock-treated worms
665 (***$p < 0.001$, Kruskal-Wallis test with *post hoc* Dunn's test). (B, C, D and E)
666 Distributions of extracted features. Duration (B), the initial value of bearing change (C),
667 the average odor concentration (D), and the average odor concentration change (E) of
668 each run (**$p < 0.01$ and ***$p < 0.001$, Kruskal-Wallis test with *post hoc* Dunn's test).
669 t_{crit} for wild type worms was 13.1. Bars represent median and first and third quartiles.

670 (F) Time course changes in ensemble averages of odor concentration (*dC*) that worms
671 experienced before the termination of runs. On average, naive and mock-treated worms
672 experienced odor decrements of about -8 nM/s until 15 s before the end of each run,
673 when the decrements started to become very close to zero at the end of the run. In
674 contrast, preexposed animals consistently experienced smaller (i.e., shallower) odor
675 decrements during runs, and the average odor concentration changes at the end of runs
676 were positive. Bars represent mean ± SEM. (G) A model relationship between odor
677 concentration change and behavioral response during navigation along the odor gradient.
678 When naive and mock-treated worms sensed a slight increase in the odor concentration,
679 which is a sign of migrating in the wrong direction, they stopped a run and started a
680 pirouette to search for a new direction. In contrast, the preexposed worms did not
681 respond to a slight increase in odor concentration, leading to longer run durations and
682 shorter pirouette durations in total, which likely contribute to the enhanced avoidance
683 distance. Numbers of worms are 25 for all the conditions, and all the statistical details
684 are described in Supplementary Table 1.
685
686 Figure 3. Sensory responses to slight odor concentration increases were reduced by
687 preexposure to the odor. (A) A schematic drawing of calcium imaging of neural activity
688 of worms under odor stimuli. Several immobilized worms were simultaneously exposed
689 to an odor flow whose concentration was changed by controlling syringe pumps. (B)
690 Responses (GCaMP/mCherry) of ASH neurons in naive (n = 25), mock-treated (n = 29),
691 and preexposed (n = 26) worms. Thick colored lines with gray shadows indicate mean ±
692 SEM, and thin lines indicate individual responses. (C) Distributions of peak values

693 during the odor-increasing phase (t = 40-80 s) shown in panel B. Bars represent median.
694 (***p < 0.001, Kruskal-Wallis test with *post hoc* Dunn's test).
695
696 Figure 4. Examples of extracted features of mutant strains. Avoidance distance (A), the
697 average velocity (B), the average migratory direction (C), and the initial odor
698 concentration (D) per run are shown. t_{crit} for each strain was 8.1 (*egl-3(n589)*), 7.2
699 (*egl-3(ok979)*), 18.1 (*dop-3(tm1356)*), 11.2 (*ocr-2(ak47)*), 17.8 (*osm-9(ky10)*), and 6.7
700 (*tax-4(p678)*). Thick bars represent statistical differences between preexposed worms
701 versus naive *and* mock-treated worms, suggesting differences caused by the odor
702 preexposure; thin bars represent statistical differences between preexposed worms
703 versus naive *or* mock-treated worms, which were not caused by the preexposure. (**p <
704 0.01 and ***p < 0.001, Kruskal-Wallis test with *post hoc* Dunn's test)
705
706 Figure 5. Experience-dependent changes in bat acoustic navigation. (A) Measurement
707 system for 3D flight trajectory of a bat during obstacle avoidance flight in a chamber.
708 (B) Representative flight trajectories of a bat in horizontal plane during repeated flight
709 in the obstacle course. The top figure combines the initial three (red) and last three
710 (blue) flight trajectories. Each behavioral feature was collected in three segments:
711 earlier, middle, and later terms. Bottom figure shows an expanded view of the earlier
712 term in the first flight. Definition of the horizontal bearing of the flight (*B_hori*),
713 distance (*R_obs*), and bearing (*B_obs*) of the bat to the nearest edge point of the
714 obstacle chain array, longitudinal directional distance to the frontal chain array (*R_x*),
715 and lateral directional distance to the inside pitch of the chains array (*R_y*) are indicated.

Time windows for the analysis of each behavioral feature were 0.1, 0.2, or 0.3 s before or when ($t = 0$) passing through the chain array. (C) A list of extracted features of bat acoustic navigation modulated by flight experience. (D) Distributions of *V(-0.3)* and *dV(-0.3)* are plotted. Bars represent median and first and third quartiles. (*$p < 0.05$, Kruskal-Wallis test with *post hoc* Dunn's test).

ACKNOWLEDGEMENTS

We thank Drs. André Brown, Katsuyoshi Matsushita, Ken-ichi Hironaka, Takuma Degawa, and the Kimura laboratory members for suggestions and comments on this work. Nematode strains were provided by the Caenorhabditis Genetics Center (funded by the NIH Office of Research Infrastructure Programs P40 OD010440) and by National Bioresource Project funded by the Ministry of Education, Culture, Sports, Science and Technology (MEXT), Japan. This work was supported by Interdisciplinary graduate school program for systematic understanding of health and disease (for S.J.Y.), by KAKENHI 25249020 and JP16H06536 (for K.H.), JP16H06542 (for S.H.), JP16H06539 (for T.M.), JP16H06545 (for K.D.K.) from the MEXT, by PRESTO JPMJPR14D8 (for S.H.) by JST, and by Osaka University Co-Creation Program (for T.M. and K.D.K.).

AUTHOR CONTRIBUTIONS

S.J.Y, T.M. and K.D.K. designed the experiments, S.J.Y, Y.I., F.H., K.F., Y.T., Y.Y., K.H., S.H. and K.D.K. performed the experiments, S.J.Y. and T.M. analyzed the data, and S.J.Y. and K.D.K. wrote the manuscript. All authors reviewed the manuscript.

740 **REFERENCES**

741 1. Alivisatos AP, et al. (2012) The Brain Activity Map Project and the Challenge of
742 Functional Connectomics. *Neuron* 74(6):970–974.

743 2. Landhuis E (2017) Neuroscience: Big brain, big data. *Nature* 541(7638):559–
744 561.

745 3. Krakauer JW, Ghazanfar AA, Gomez-Marin A, MacIver MA, Poeppel D (2017)
746 Neuroscience Needs Behavior: Correcting a Reductionist Bias. *Neuron*
747 93(3):480–490.

748 4. Gomez-Marin A, Paton JJ, Kampff AR, Costa RM, Mainen ZF (2014) Big
749 behavioral data: psychology, ethology and the foundations of neuroscience. *Nat*
750 *Neurosci* 17(11):1455–1462.

751 5. Anderson DJ, Perona P (2014) Toward a Science of Computational Ethology.
752 *Neuron* 84(1):18–31.

753 6. Bishop CM (2006) *Pattern Recognition and Machine Learning* (Springer
754 Verlag).

755 7. Vogelstein JT, et al. (2014) Discovery of Brainwide Neural-Behavioral Maps via
756 Multiscale Unsupervised Structure Learning. *Science* 344(6182):386–392.

757 8. Kabra, M., Robie, A. A., Rivera-Alba, M., Branson, S., & Branson, K. (2013).
758 JAABA: Interactive machine learning for automatic annotation of animal
759 behavior. *Nat Meth*, *10*(1), 64–67.

760 9. Branson K, Robie AA, Bender J, Perona P, Dickinson MH (2009)
761 High-throughput ethomics in large groups of *Drosophila*. *Nat Meth* 6(6):451–
762 457.

763 10. Dankert H, Wang L, Hoopfer ED, Anderson DJ, Perona P (2009) Automated
764 monitoring and analysis of social behavior in *Drosophila*. *Nat Meth* 6(4):297–
765 303.

766 11. Baek J-H, Cosman P, Feng Z, Silver J, Schafer WR (2002) Using machine vision
767 to analyze and classify *Caenorhabditis elegans* behavioral phenotypes
768 quantitatively. *J Neurosci Methods* 118(1):9–21.

769 12. Brown AEX, Yemini EI, Grundy LJ, Jucikas T, Schafer WR (2013) A dictionary
770 of behavioral motifs reveals clusters of genes affecting *Caenorhabditis elegans*
771 locomotion. *Proc Natl Acad Sci USA* 110(2):791–796.

772 13. Stephens GJ, Johnson-Kerner B, Bialek W, Ryu WS (2008) Dimensionality and
773 Dynamics in the Behavior of *C. elegans*. *PLoS Comput Biol* 4(4):e1000028.

774 14. Lockery SR (2011) The computational worm: spatial orientation and its neuronal
775 basis in *C. elegans*. *Curr Opin Neurobiol* 21(5):782–790.

776 15. Suzuki H, et al. (2008) Functional asymmetry in *Caenorhabditis elegans* taste
777 neurons and its computational role in chemotaxis. *Nature* 454(7200):114–117.

778 16. Chronis N, Zimmer M, Bargmann CI (2007) Microfluidics for in vivo imaging of
779 neuronal and behavioral activity in *Caenorhabditis elegans*. *Nat Meth* 4(9):727–
780 731.

781 17. Clark DA, Gabel CV, Gabel H, Samuel ADT (2007) Temporal activity patterns
782 in thermosensory neurons of freely moving *Caenorhabditis elegans* encode
783 spatial thermal gradients. *J Neurosci* 27(23):6083–6090.

784 18. Kimura KD, Miyawaki A, Matsumoto K, Mori I (2004) The *C. elegans*
785 Thermosensory Neuron AFD Responds to Warming. *Curr Biol* 14(14):1291–
786 1295.

787 19. Tanimoto Y, et al. (2017) Calcium dynamics regulating the timing of
788 decision-making in *C. elegans*. *eLife* 6:13819.

789 20. Larsch J, Ventimiglia D, Bargmann CI, Albrecht DR (2013) High-throughput
790 imaging of neuronal activity in *Caenorhabditis elegans*. *Proc Natl Acad Sci USA*
791 110(45):E4266–73.

792 21. Yemini E, Jucikas T, Grundy LJ, Brown AEX, Schafer WR (2013) A database of
793 *Caenorhabditis elegans* behavioral phenotypes. *Nat Meth* 10(9):877–879.

22. Quinlan JR (1986) Induction of Decision Trees. *Mach Learn* 1(1):81–106.

23. Brenner S (1974) The genetics of *Caenorhabditis elegans*. *Genetics* 77(1):71–94.

24. Kimura KD, Fujita K, Katsura I (2010) Enhancement of odor avoidance regulated by dopamine signaling in *Caenorhabditis elegans*. *J Neurosci* 30(48):16365–16375.

25. Yamazoe-Umemoto A, Fujita K, Iino Y, Iwasaki Y, Kimura KD (2015) Modulation of different behavioral components by neuropeptide and dopamine signalings in non-associative odor learning of *Caenorhabditis elegans*. *Neurosci Res* 99:22–33.

26. Pierce-Shimomura JT, Morse TM, Lockery SR (1999) The fundamental role of pirouettes in *Caenorhabditis elegans* chemotaxis. *J Neurosci* 19(21):9557–9569.

27. Yamada Y, Hiryu S, Watanabe Y (2016) Species-specific control of acoustic gaze by echolocating bats, Rhinolophus ferrumequinum nippon and Pipistrellus abramus, during flight. *J Comp Physiol A* 202(11):791–801.

28. Gorelik R, Gautreau A (2014) Quantitative and unbiased analysis of directional persistence in cell migration. *Nat Protoc* 9(8):1931–1943.

29. Iino Y, Yoshida K (2009) Parallel use of two behavioral mechanisms for chemotaxis in *Caenorhabditis elegans*. *J Neurosci* 29(17):5370–5380.

30. Quinlan JR (1992) *C4.5* (Morgan Kaufmann, San Mateo).

31. Frank E, Hall MA, Witten IH (2016) The WEKA Workbench (Online Appendix). *Data Mining* (Morgan Kaufmann). Forth Edition.

32. Tian L, et al. (2009) Imaging neural activity in worms, flies and mice with improved GCaMP calcium indicators. *Nat Meth* 6(12):875–881.

33. Shaner NC, et al. (2004) Improved monomeric red, orange and yellow fluorescent proteins derived from *Discosoma sp.* red fluorescent protein. *Nat Biotech* 22(12):1567–1572.

34. Lewis JA, Wu CH, Berg H, Levine JH (1980) The genetics of levamisole resistance in the nematode *Caenorhabditis elegans*. *Genetics* 95(4):905–928.

35. Zheng Y (2015) Trajectory Data Mining. *ACM Trans Intell Syst Technol* 6(3):1–41.

36. Louis M, Huber T, Benton R, Sakmar TP, Vosshall LB (2008) Bilateral olfactory sensory input enhances chemotaxis behavior. *Nat Neurosci* 11(2):187–199.

37. Kato S, Xu Y, Cho CE, Abbott LF, Bargmann CI (2014) Temporal responses of *C. elegans* chemosensory neurons are preserved in behavioral dynamics. *Neuron* 81(3):616–628.

38. Teghtsoonian R (1971) On the exponents in Stevens' law and the constant in Ekman's law. *Psycho Rev* 78(1):71–80.

39. Kaplan JM (1996) Sensory signaling in *Caenorhabditis elegans*. *Curr Opin Neurobiol* 6(4):494–499.

40. Bargmann CI (2006) Chemosensation in *C. elegans*. *WormBook*:1–29.

41. Kass J, Jacob TC, Kim P, Kaplan JM (2001) The EGL-3 proprotein convertase regulates mechanosensory responses of *Caenorhabditis elegans*. *J Neurosci* 21(23):9265–9272.

42. Suo S, Ishiura S, Van Tol HHM (2004) Dopamine receptors in *C. elegans*. *Eur J Pharmacol* 500(1-3):159–166.

43. Tobin D, et al. (2002) Combinatorial expression of TRPV channel proteins defines their sensory functions and subcellular localization in *C. elegans* neurons. *Neuron* 35(2):307–318.

44. Colbert HA, Smith TL, Bargmann CI (1997) OSM-9, a novel protein with structural similarity to channels, is required for olfaction, mechanosensation, and olfactory adaptation in *Caenorhabditis elegans*. *J Neurosci* 17(21):8259–8269.

45. Komatsu H, Mori I, Rhee JS, Akaike N, Ohshima Y (1996) Mutations in a cyclic nucleotide-gated channel lead to abnormal thermosensation and chemosensation in *C. elegans*. *Neuron* 17(4):707–718.

46. Li C, Kim K (2008) Neuropeptides. *WormBook*:1–36.

47. Husson SJ, Clynen E, Baggerman G, Janssen T, Schoofs L (2006) Defective processing of neuropeptide precursors in *Caenorhabditis elegans* lacking proprotein convertase 2 (KPC-2/EGL-3): mutant analysis by mass spectrometry. *J Neurochem* 98(6):1999–2012.

48. Chase DL, Koelle MR (2007) Biogenic amine neurotransmitters in *C. elegans*. *WormBook*:1–15.

49. Moss CF, Surlykke A (2010) Probing the natural scene by echolocation in bats. *Front Behav Neurosci* 4. doi:10.3389/fnbeh.2010.00033.

50. Hong W, et al. (2015) Automated measurement of mouse social behaviors using depth sensing, video tracking, and machine learning. *Proc Natl Acad Sci USA* 112(38):E5351–E5360.

51. Gershow M, et al. (2012) Controlling airborne cues to study small animal navigation. *Nat Meth* 9(3):290–296.

52. Albrecht DR, Bargmann CI (2011) High-content behavioral analysis of *Caenorhabditis elegans* in precise spatiotemporal chemical environments. *Nat Meth* 8(7):599–605.

53. Burges CJC (1998) A tutorial on support vector machines for pattern recognition. *Data Mining and Knowledge Discovery* 2(2):121–167.

54. LeCun Y, Bengio Y, Hinton G (2015) Deep learning. *Nature* 521(7553):436–444.

Table 1. A list of behavioral features used for worms' olfactory navigation

Parameters	Definition
RunNum	Number of a run
RunTime	Start time of a run
RunDur	Duration of a run
PirDur	Duration of the previous pirouette
V_Ave	Average velocity during a run
V_Ini	Velocity at run initiation
V_Ter	Velocity at run termination
dV_Ave	Average acceleration during a run
dV_Ini	Acceleration at run initiation
dV_Ter	Acceleration at run termination
B_Ave	Bearing of migratory vector throughout a run
B_Ini	Bearing at run initiation
B_Ter	Bearing at run termination
dB_Ave	Average temporal changes in bearing
dB_Ini	Temporal changes in bearing at run initiation
dB_Ter	Temporal changes in bearing at run termination
C_Ave	Average odor concentration during a run
C_Ini	Odor concentration at run initiation
C_Ter	Odor concentration at run termination
dC_Ave	Average temporal changes in odor concentration during a run
dC_Ini	Temporal changes in odor concentration at run initiation
dC_Ter	Temporal changes in odor concentration at run termination
Dir_Ave	Average directionality ratio
Dir_Ini	Directionality ratio at run initiation
Dir_Ter	Directionality ratio at run termination
WV	Curving rate of a run
RunDurΔ	Current *RunDur* minus the previous *RunDur*
PirDurΔ	Current *PirDur* minus the previous *PirDur*
WVΔ	Current *WV* minus the previous *WV*
X_AveΔAve	Current *Ave* minus the previous *Ave*
X_AveΔIni	Current *Ave* minus the previous *Ini*
X_AveΔTer	Current *Ave* minus the previous *Ter*
X_IniΔAve	Current *Ini* minus the previous *Ave*
X_IniΔIni	Current *Ini* minus the previous *Ini*
X_IniΔTer	Current *Ini* minus the previous *Ter*
X_TerΔAve	Current *Ter* minus the previous *Ave*
X_TerΔIni	Current *Ter* minus the previous *Ini*
X_TerΔTer	Current *Ter* minus the previous *Ter*
(*X* = *V, dV, B, dB, C, dC, Dir*)	

Table 2. Extracted features of worms' olfactory navigation modulated by prior odor experience

naive vs pre-exp		mock vs pre-exp	
V_Ave	0.1796	***C_Ter***	0.1337
Run_Dur	0.1558	***C_Ave***	0.0998
dB_Ini	0.1349	***C_Ini***	0.0932
C_IniΔAve	0.1230	***dC_Ave***	0.0854
C_IniΔIni	0.1230	*dC_Ini*	0.0810
dB_TerΔIni	0.1191	***dC_Ter***	0.0749
dB_AveΔIni	0.1013	*dC_IniΔTer*	0.0722
C_Ave	0.0983	*dC_TerΔIni*	0.0490
C_Ter	0.0942	*dV_AveΔIni*	0.0478
dB_IniΔTer	0.0924	*dV_Ini*	0.0478
C_Ini	0.0914	*dV_Ave*	0.0364
dB_IniΔAve	0.0839	***Run_Dur***	0.0352
V_AveΔAve	0.0815	***dB_Ini***	0.0342
dC_Ter	0.0810	***dB_TerΔIni***	0.0304
Run_DurΔ	0.0785	***dB_AveΔIni***	0.0298
dC_Ave	0.0547		
C_AveΔTer	0.0394		
Pir_Dur	0.0326		

Bold letters indicate features shared between the two comparisons.

878 **Table 3. Summary of extracted features of wild-type and mutant strains that are modulated by prior odor experience**

strain	*RunDur*	*V_Ave*	*V_Ini*	*V_Ter*	*B_Ter*	*dB_Ini*	*C_Ave*	*C_Ini*	*C_Ter*	*dC_Ave*	*dC_Ter*	*Dir_Ave*	*RunNum*
wild-type	up					down	down	down	down	up	up		
egl-3(n589)							up	up	up				
egl-3(ok979)		down	down	down		down	up	up	up				
dop-3(tm1356)	up	down		down	up					up	up	down	
ocr-2(ak47)		up		up	up								
osm-9(ky10)	up	up		up									
tax-4(p678)													up

879 Only features with statistical differences between preexposed worms versus naive *and* mock-treated worms are shown.

880

Table 4. A list of behavioral features used for bats' acoustic navigation

Parameters	Definition
V(t)	Fight velocity in 3D space
dV(t)	Flight acceleration in 3D space
B_hori(t)	Absolut bearing of the flight vector in a horizontal plane
dB_hori(t)	Temporal change in bearing of the flight vector in a horizontal plane
ddB_hori(t)	Temporal acceleration in bearing of the flight vector in a horizontal plane
B_vert(t)	Absolut bearing of the flight vector in a vertical plane
B_obs(t)	Absolute bearing to the edge point of the nearest chain array
R_obs(t)	Distance from the bat to the edge point of the nearest chain array
R_x(t)	Longitudinal directional distance to the frontal chain array
R_y(t)	Lateral directional distance to the inside pitch of the chain array
dH(t)	Temporal change in flight height

t = -0.3, -0.2, -0.1, or 0 s. *B_obs(t)* and *R_x(t)* were not calculated for t = 0.

Figure 1

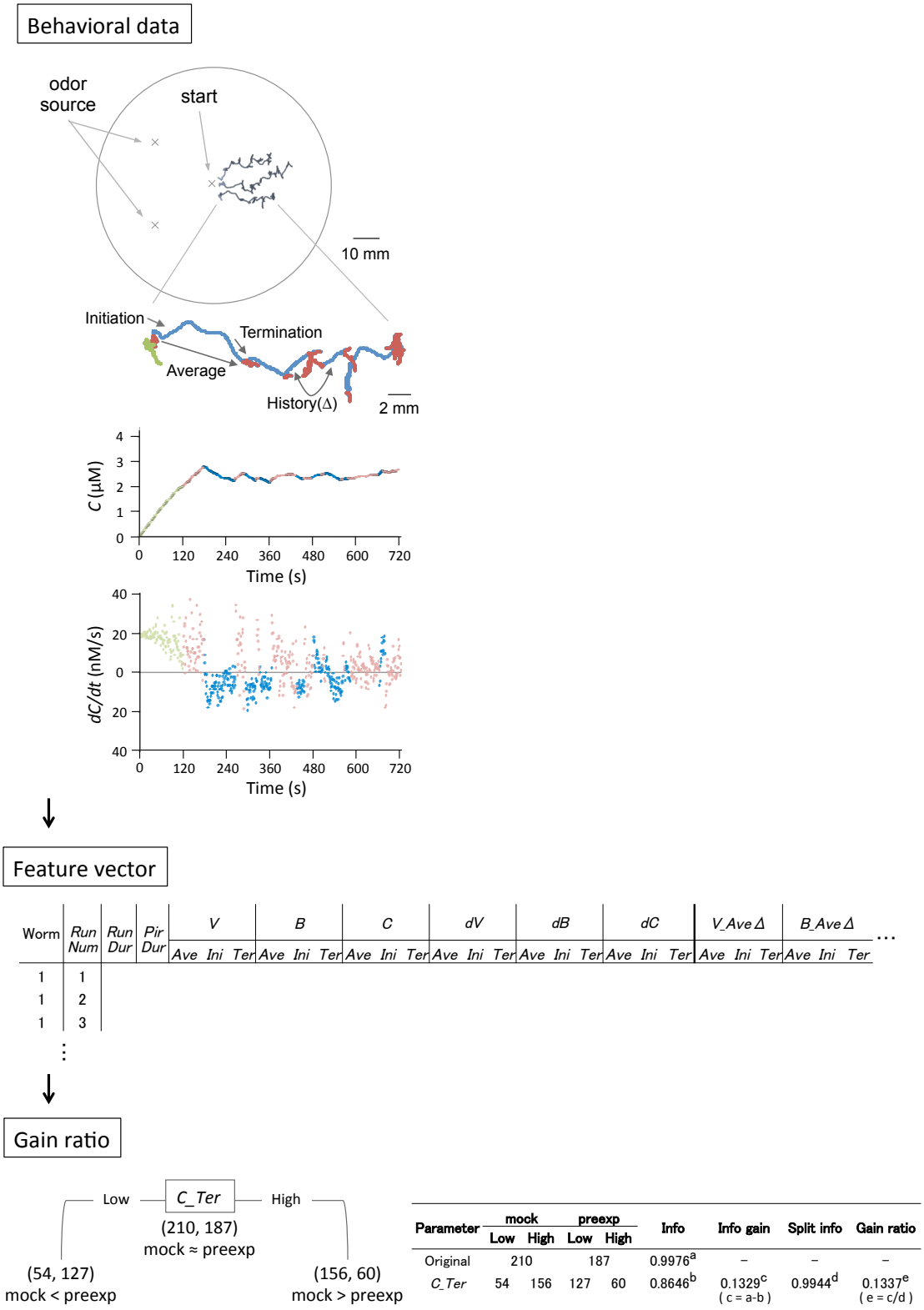

Parameter	mock Low	mock High	preexp Low	preexp High	Info	Info gain	Split info	Gain ratio
Original	210		187		0.9976[a]	–	–	–
C_Ter	54	156	127	60	0.8646[b]	0.1329[c] (c = a-b)	0.9944[d]	0.1337[e] (e = c/d)

Figure 2

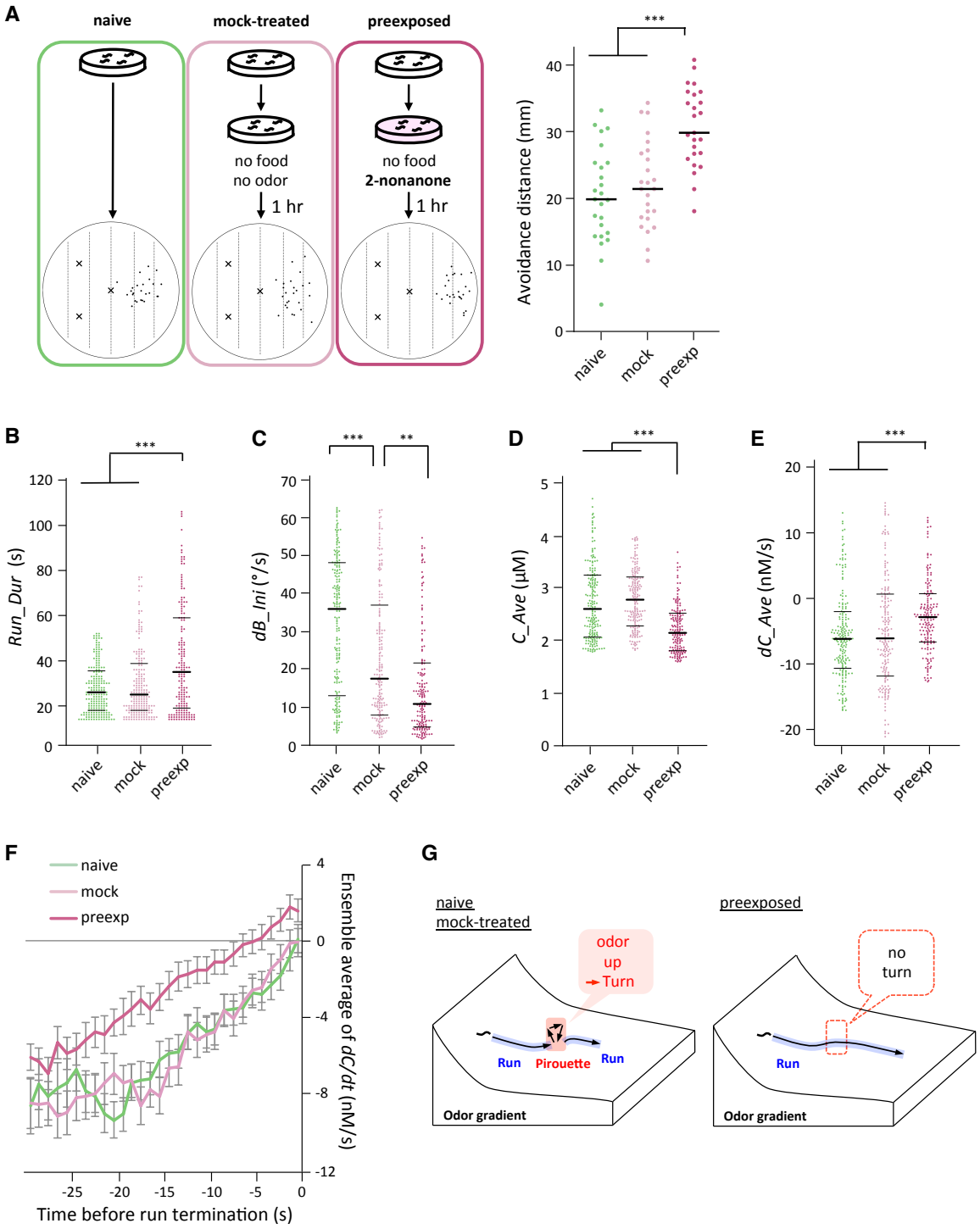
A
naive
mock-treated
preexposed
no food
no odor
1 hr
no food
2-nonanone
1 hr
Avoidance distance (mm)
***
naive
mock
preexp
B
Run_Dur (s)
***
C
dB_Ini (°/s)
***
**
D
C_Ave (µM)
***
E
dC_Ave (nM/s)
***
F
naive
mock
preexp
Ensemble average of dC/dt (nM/s)
Time before run termination (s)
G
naive
mock-treated
odor
up
Turn
Run
Pirouette
Run
Odor gradient
preexposed
no
turn
Run
Odor gradient

Figure 3

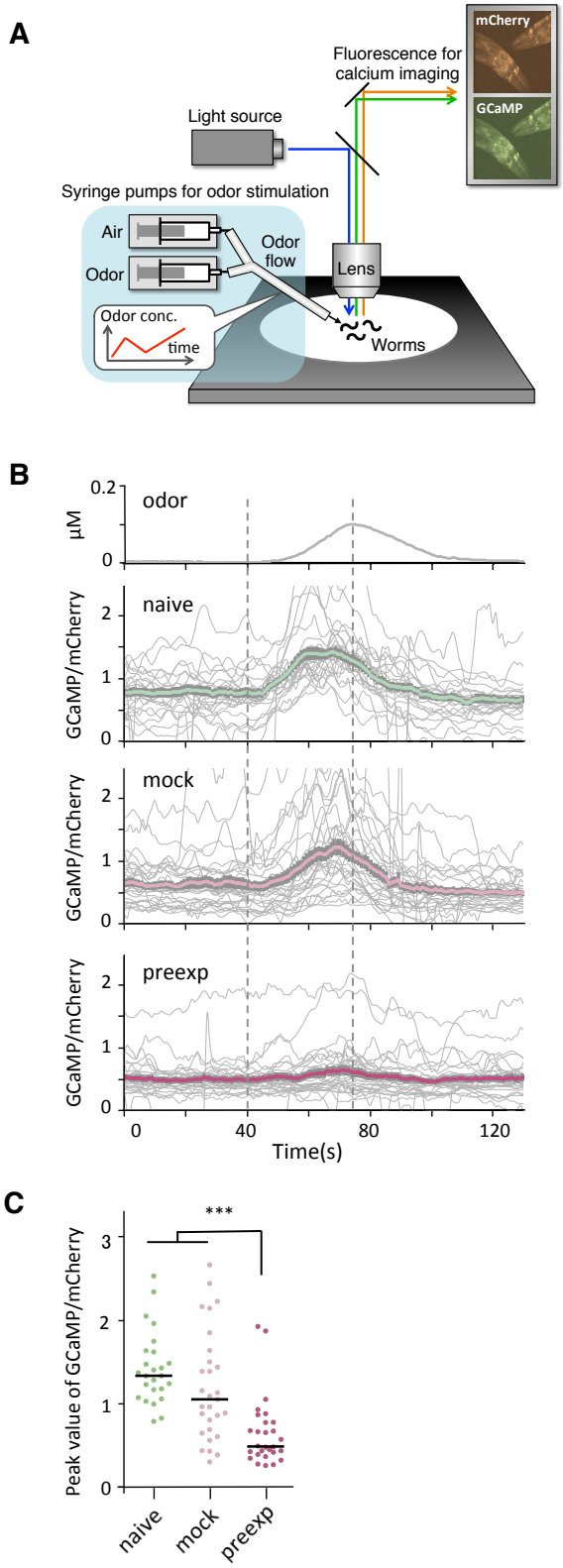
A
mCherry
GCaMP
Fluorescence for calcium imaging
Light source
Syringe pumps for odor stimulation
Air
Odor
Odor flow
Lens
Odor conc.
time
Worms
B
odor
μM
0.2
0
naive
mock
preexp
GCaMP/mCherry
2
1
0
0
40
80
120
Time(s)
C
***
Peak value of GCaMP/mCherry
3
2
1
0
naive
mock
preexp

Figure 4

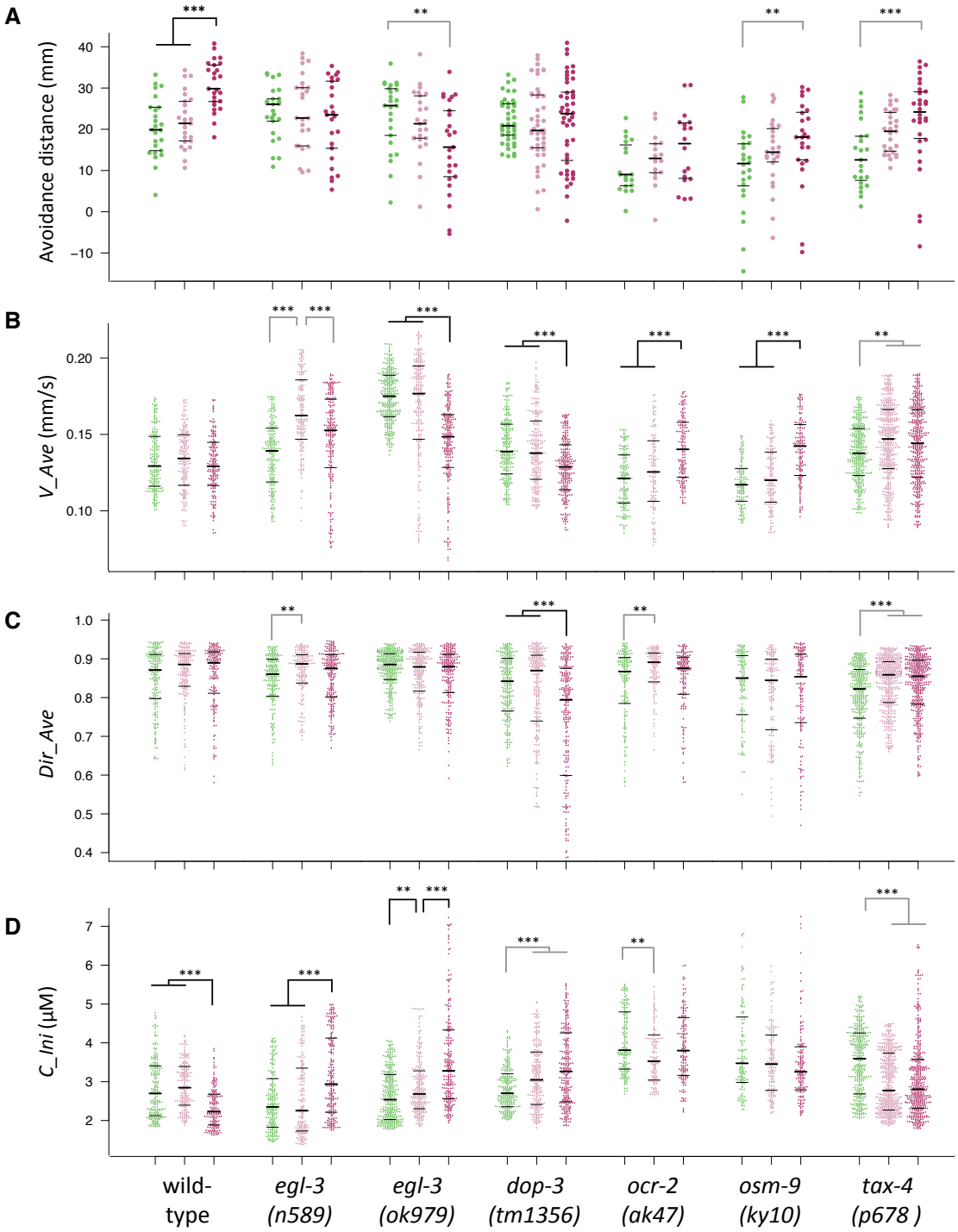
A
Avoidance distance (mm)
B
V_Ave (mm/s)
C
Dir_Ave
D
C_Ini (μM)
wild-type
egl-3 (n589)
egl-3 (ok979)
dop-3 (tm1356)
ocr-2 (ak47)
osm-9 (ky10)
tax-4 (p678)

Figure 5

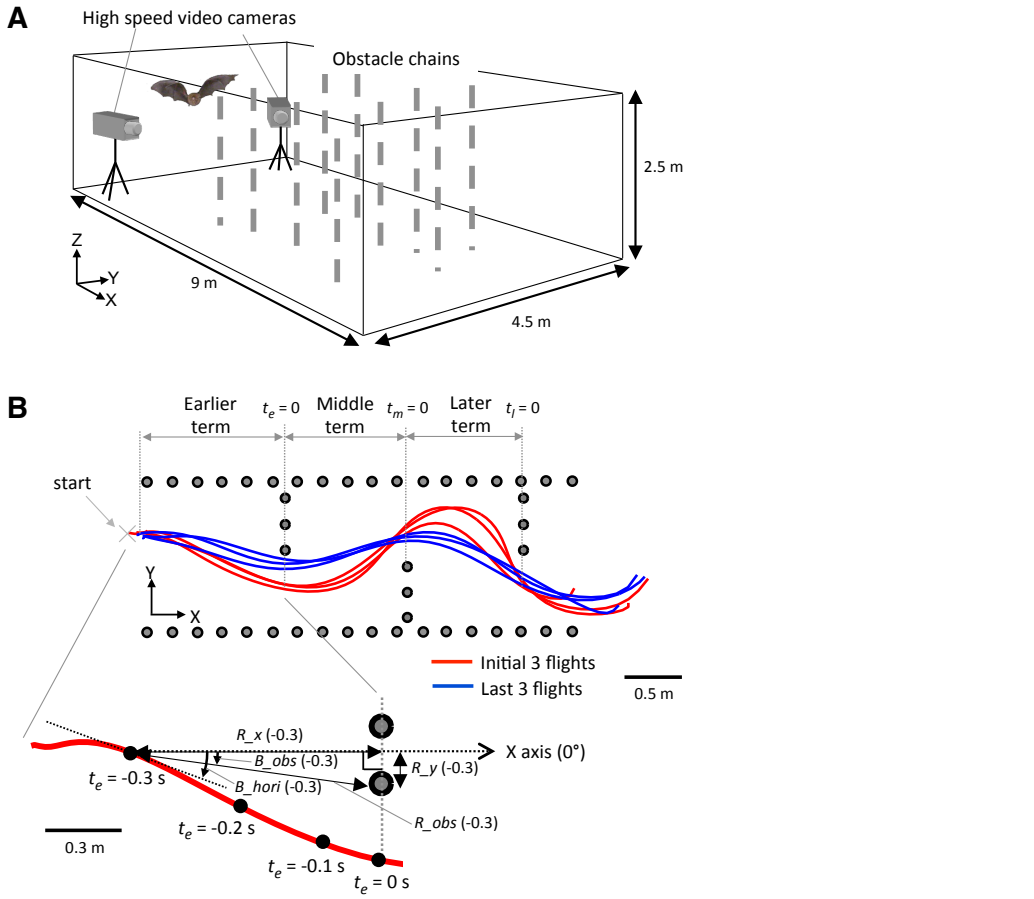

C

Features	Gain ratio
R_x (-0.3)	0.373
R_obs (-0.3)	0.352
V (-0.3)	0.312
V (-0.2)	0.294
R_x (-0.2)	0.294
R_obs (-0.2)	0.294
B_hori (-0.3)	0.292
B_hori (-0.2)	0.219
ddB_hori (-0.3)	0.209

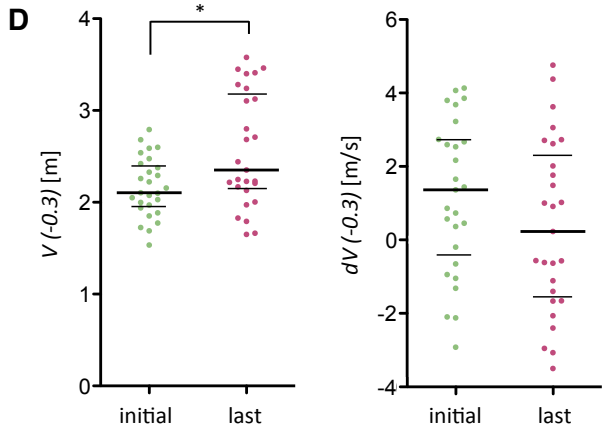

Supplementary Table 1

Supplementary Table 1. Detailed results of statistical tests.

Figure	Parameter	Number of naive	Number of mock	Number of preexp.	Unit of number	Multiple test	df value of multiple test	p value of multiple test	Other result of multiple test	Post-hock test	df value of post-hock test	p value of post-hock test	Other result of post-hock test
2A, 4A	Avoidance distance of N2	25	25	25	animals	Kruskal-Wallis test	2	<0.0001(***)	24.451	Dunn's test	1	naive vs mock: 0.7621(ns) naive vs preexposure: <0.0001(***) mock vs preexposure: 0.0001(***)	z = 0.6619 z = 4.5747 z = 3.9128
2B	Run duration of N2	219	210	187	runs	Kruskal-Wallis test	2	<0.0001(***)	18.76	Dunn's test	1	naive vs mock: 1(ns) naive vs preexposure: <0.0001(***) mock vs preexposure: 0.0006(***)	z = -0.4269 z = -3.9959 z = -3.547
2C	Initial dBearing of N2	219	210	187	runs	Mardia-Watson-Wheeler test	2	<0.0001(***)	64.69	Mardia-Watson-Wheeler test	1	naive vs mock: <0.0001(***) naive vs preexposure: <0.0001(***) mock vs preexposure: 0.002(**)	W = 26.305 W = 59.795 W = 12.007
2D	Average Conc. of N2	219	210	187	runs	Kruskal-Wallis test	2	<0.0001(***)	68.69	Dunn's test	1	naive vs mock: 0.1351(ns) naive vs preexposure: <0.0001(***) mock vs preexposure: <0.0001(***)	z = -1.6951 z = 6.3349 z = 7.9016
2E	Averege dConc. of N2	219	210	187	runs	Kruskal-Wallis test	2	0.0003(***)	16.56	Dunn's test	1	naive vs mock: 0.3202(ns) naive vs preexposure: <0.0001(***) mock vs preexposure: 0.0085(**)	z = -1.2441 z = -4.001 z = -2.7671
3C	Peak value of GCaMP3/mCherry	25	29	28	animals	Kruskal-Wallis test	2	<0.0001(***)	30.11	Dunn's test	1	naive vs mock: 0.0949(ns) naive vs preexposure: <0.0001(***) mock vs preexposure: 0.0004(***)	z = 1.8571 z = 5.3589 z = 3.6525
4A	Avoidance distance of *egl-3(n589)*	25	25	25	animals	Kruskal-Wallis test	2	0.7763(ns)	0.51	Dunn's test	1	-	-
4A	Avoidance distance of *egl-3(ok979)*	25	25	25	animals	Kruskal-Wallis test	2	0.0128(*)	8.72	Dunn's test	1	naive vs mock: 0.3924(ns) naive vs preexposure: 0.0051(**) mock vs preexposure: 0.1069(ns)	z = -1.1226 z = -2.9265 z = -1.8039
4A	Avoidance distance of *dop-3(tm1356)*	46	46	47	animals	Kruskal-Wallis test	2	0.8196(ns)	0.40	Dunn's test	1	-	-
4A	Avoidance distance of *ocr-2(ak47)*	19	16	18	animals	Kruskal-Wallis test	2	0.2001(ns)	3.22	Dunn's test	1	-	-
4A	Avoidance distance of *osm-9(ky10)*	24	26	24	animals	Kruskal-Wallis test	2	0.0191(*)	7.91	Dunn's test	1	naive vs mock: 0.1625(ns) naive vs preexposure: 0.0075(**) mock vs preexposure: 0.3141(ns)	z = 1.6058 z = 2.8055 z = 1.2552
4A	Avoidance distance of *tax-4(p678)*	23	29	30	animals	Kruskal-Wallis test	2	0.0008(***)	14.39	Dunn's test	1	naive vs mock: 0.0506(ns) naive vs preexposure: 0.0002(***) mock vs preexposure: 0.1175(ns)	z = 2.1232 z = 3.7932 z = 1.7605
4B	Average speed of N2	219	210	187	runs	Kruskal-Wallis test	2	0.2796(ns)	2.55	Dunn's test	1	-	-
4B	Average speed of *egl-3(n589)*	227	194	235	runs	Kruskal-Wallis test	2	<0.0001(***)	80.44	Dunn's test	1	naive vs mock: <0.0001(***) naive vs preexposure: <0.0001(***) mock vs preexposure: <0.0001(***)	z = -8.9653 z = -4.5544 z = 4.6671
4B	Average speed of *egl-3(ok979)*	370	260	252	runs	Kruskal-Wallis test	2	<0.0001(***)	137.51	Dunn's test	1	naive vs mock: 0.3296(ns) naive vs preexposure: <0.0001(***) mock vs preexposure: <0.0001(***)	z = 1.2272 z = 11.1444 z = 9.1734
4B	Average speed of *dop-3(tm1356)*	276	266	279	runs	Kruskal-Wallis test	2	<0.0001(***)	39.19	Dunn's test	1	naive vs mock: 0.6155(ns) naive vs preexposure: <0.0001(***) mock vs preexposure: <0.0001(***)	z = 0.8234 z = 5.795 z = 4.9154
4B	Average speed of *ocr-2(ak47)*	180	142	168	runs	Kruskal-Wallis test	2	<0.0001(***)	50.52	Dunn's test	1	naive vs mock: 0.075(ns) naive vs preexposure: <0.0001(***) mock vs preexposure: <0.0001(***)	z = -1.9599 z = -6.9657 z = -4.6254
4B	Average speed of *osm-9(ky10)*	147	175	160	runs	Kruskal-Wallis test	2	<0.0001(***)	66.85	Dunn's test	1	naive vs mock: 0.2053(ns) naive vs preexposure: <0.0001(***) mock vs preexposure: <0.0001(***)	z = -1.4875 z = -7.5979 z = -6.4146
4B	Average speed of *tax-4(p678)*	402	531	473	runs	Kruskal-Wallis test	2	<0.0001(***)	20.69	Dunn's test	1	naive vs mock: <0.0001(***) naive vs preexposure: 0.0019(**) mock vs preexposure: 0.3492(ns)	z = -4.456 z = -3.2307 z = 1.1931
4C	Average directionality ratio of N2	219	210	187	runs	Kruskal-Wallis test	2	0.2781(ns)	2.56	Dunn's test	1	-	-
4C	Average directionality ratio of *egl-3(n589)*	227	194	235	runs	Kruskal-Wallis test	2	0.0042(**)	10.96	Dunn's test	1	naive vs mock: 0.0014(**) naive vs preexposure: 0.1115(ns) mock vs preexposure: 0.1585(ns)	z = -3.3036 z = -1.7844 z = 1.6179
4C	Average directionality ratio of *egl-3(ok979)*	370	260	252	runs	Kruskal-Wallis test	2	0.1357(ns)	4.00	Dunn's test	1	-	-
4C	Average directionality ratio of *dop-3(tm1356)*	276	266	279	runs	Kruskal-Wallis test	2	<0.0001(***)	38.61	Dunn's test	1	naive vs mock: 1(ns) naive vs preexposure: <0.0001(***) mock vs preexposure: <0.0001(***)	z = -0.3986 z = 5.1836 z = 5.5349
4C	Average directionality ratio of *ocr-2(ak47)*	180	142	168	runs	Kruskal-Wallis test	2	0.0135(*)	8.62	Dunn's test	1	naive vs mock: 0.0062(**) naive vs preexposure: 0.6577(ns) mock vs preexposure: 0.0541(ns)	z = -2.8694 z = -0.7747 z = 2.0962
4C	Average directionality ratio of *osm-9(ky10)*	147	175	160	runs	Kruskal-Wallis test	2	0.6949(ns)	0.73	Dunn's test	1	-	-
4C	Average directionality ratio of *tax-4(p678)*	402	531	473	runs	Kruskal-Wallis test	2	<0.0001(***)	37.08	Dunn's test	1	naive vs mock: <0.0001(***) naive vs preexposure: <0.0001(***) mock vs preexposure: 1(ns)	z = -5.4554 z = -5.2773 z = 0.0423
4D	Initial Conc. of N2	219	210	187	runs	Kruskal-Wallis test	2	<0.0001(***)	57.75	Dunn's test	1	naive vs mock: 0.1381(ns) naive vs preexposure: <0.0001(***) mock vs preexposure: <0.0001(***)	z = -1.6846 z = 5.7215 z = 7.284
4D	Initial Conc. of *egl-3(n589)*	227	194	235	runs	Kruskal-Wallis test	2	<0.0001(***)	48.82	Dunn's test	1	naive vs mock: 1(ns) naive vs preexposure: <0.0001(***) mock vs preexposure: <0.0001(***)	z = 0.0374 z = -6.0955 z = -5.8855
4D	Initial Conc. of *egl-3(ok979)*	370	260	252	runs	Kruskal-Wallis test	2	<0.0001(***)	83.00	Dunn's test	1	naive vs mock: 0.002(**) naive vs preexposure: <0.0001(***) mock vs preexposure: <0.0001(***)	z = -3.2048 z = -9.0932 z = -5.4678
4D	Initial Conc. of *dop-3(tm1356)*	276	266	279	runs	Kruskal-Wallis test	2	<0.0001(***)	30.83	Dunn's test	1	naive vs mock: 0.001(***) naive vs preexposure: <0.0001(***) mock vs preexposure: 0.064(ns)	z = -3.4101 z = -5.4972 z = -2.0269
4D	Initial Conc. of *ocr-2(ak47)*	180	142	168	runs	Kruskal-Wallis test	2	0.0151(*)	8.38	Dunn's test	1	naive vs mock: 0.0057(**) naive vs preexposure: 0.2973(ns) mock vs preexposure: 0.1517(ns)	z = 2.8947 z = 1.2868 z = -1.6393
4D	Initial Conc. of *osm-9(ky10)*	147	175	160	runs	Kruskal-Wallis test	2	0.0637(ns)	5.51	Dunn's test	1	-	-
4D	Initial Conc. of *tax-4(p678)*	402	531	473	runs	Kruskal-Wallis test	2	<0.0001(***)	76.84	Dunn's test	1	naive vs mock: <0.0001(***) naive vs preexposure: <0.0001(***) mock vs preexposure: 0.8193(ns)	z = 8.0792 z = 7.3115 z = -0.6035

Figure	Parameter	Number of Groups	Number of initial	Number of last	Unit of number	Statistical tests used	p value	Other result
5D	Fight velocity in 3D space at t=−0.3	2	27	27	flights	Mann–Whitney test	0.0234(*)	Mann-Whitney U = 233.0
5D	Flight acceleration in 3D space at t=−0.3	2	27	27	flights	Mann–Whitney test	0.2326(ns)	Mann-Whitney U = 295.0